THE ASTROPHYSICAL JOURNAL, Vol. 158, October 1969

LARGE-SCALE SHOCK FORMATION IN SPIRAL GALAXIES AND ITS IMPLICATIONS ON STAR FORMATION

W. W. ROBERTS*
Massachusetts Institute of Technology
Received 1969 February 3

ABSTRACT

The dynamical problems of shock formation and star formation in normal spiral galaxies are investigated. The motion considered is that of the continuum of turbulent gas composing the gaseous disk moving in a gravitational field consisting of a two-armed spiral field superposed on the Schmidt model for the Milky Way system. The possible existence of a stationary two-armed spiral shock pattern is demonstrated. It is suggested that galactic shock waves may very well form the triggering mechanism for the gravitational collapse of gas clouds, leading to star formation. If an upper bound of 30 million years is assumed for the process of formation and evolution of relatively massive stars initiated at the shock, it is shown that the possible locations of the regions of luminous, newly born stars and the H II regions lie on the inner side of each observable gaseous spiral arm of H I, extending from the sharp H I peak at the shock on the inner edge to approximately the center of the arm, in general agreement with observations.

I. INTRODUCTION

Many spiral galaxies have multiple spiral arms; however, two principal arms can generally be traced to the central region and sometimes to the very center of the system (see Sandage 1961). Often the spiral arms show a very high resolution into "knots" that are generally interpreted as H II regions and associations of stars. While the young stars practically always appear in stellar associations, the young stellar associations with their corresponding brilliant H II regions often occur in chains and spiral arcs within the larger grand design of spiral structure. The contiguity of H II regions and spiral arms was first recognized by Baade and Mayall (1951) in their study of the H II regions of M31. It was Morgan, Sharpless, and Osterbrock (1952) who first detected spiral structure in our Galaxy and who showed that the young stars and H II regions appear like strings of beads. In recent observational studies of our Galaxy, Westerhout (1968) has found that the young stellar associations and brilliant H II regions actually lie along the inner sides of the observed gaseous spiral arms. In view of these observational studies, a basic problem stands out, namely, what physical mechanism could trigger star formation along a grand design of spiral structure in such an orderly fashion.

M. S. Roberts (1967) has shown for a number of Sc-type galaxies that the circumferential bands with highest H I distribution not only do not coincide with but lie significantly outside the circumferential bands containing the most prominent newly born stars and H II regions. It would seem obvious a priori that star formation would most probably take place in those regions where the mass of neutral hydrogen is the largest. To have little or no star formation in the regions of highest H I distribution seems indeed perplexing. This is just one further aspect of star formation that must be considered.

a) Grand Design of Spiral Structure

Two different spiral theories have been suggested to account for the grand design feature. The first associates each spiral arm with a specified body of matter throughout the course of the arm's evolution. The winding dilemma associated with the disrupting influence of differential rotation is an uncomfortable difficulty arising out of this theory.

* Now at the University of Virginia, Charlottesville.

The second theory is the density-wave theory of spiral structure that was first proposed by the late B. Lindblad (see Lindblad and Langebartel 1953; Lindblad 1963). Since he placed emphasis on the properties of individual stellar orbits rather than on the behavior of stellar collective modes, it was difficult to demonstrate a convincing case. P. O. Lindblad (1960, 1962) studied the collective modes by extensive numerical calculation of the orbits of a number of stars. Although density waves of a spiral form were found, they were rather transient and not quasi-stationary. On the other hand, by means of an asymptotic analysis, Lin and Shu (1964, 1966) developed a density-wave theory in which the wave pattern shows a spiral structure that remains quasi-stationary in a frame of reference rotating around the center of the galaxy at a definite angular speed. In this theory, the persistence of a regular grand design may be maintained despite the presence of differential rotation. In addition, it is shown that only a two-armed spiral pattern is possible when the basic rotation curve is similar to that of the Milky Way system.

b) Large-Scale Galactic Shocks

The presence of a marked grand design of spiral structure in many disk-shaped galaxies signifies an even more marked and narrow region for the initiation of star formation within the gaseous spiral arms of the grand design. In the density-wave theory, this is indeed a very urgent problem to be explained, for the gas stays inside the spiral arm for a relatively short period of time. In the linear theory, the gas concentration in a density wave extends over a broad region and could not be expected to provide a sufficiently rapid triggering mechanism to produce narrow spiral strips of newly born luminous stars. We are therefore led to infer the presence of large-scale "galactic shocks" that would be capable of triggering star formation in such narrow spiral strips over the disk.

We should distinguish the large-scale galactic shocks from the various types of small-scale shock waves previously considered for the interstellar medium (see Axford 1961; Goldsworthy 1961; Kahn 1962, 1968*a;* Kahn and Dyson 1965; Wentzel 1966; Mathews 1965; Lasker 1966*a,b;* Field *et al.* 1968). All these investigations actually consider small-scale shocks in a relatively small region of the interstellar medium (with a typical scale of at most 10 pc and containing at most a few stars and a few gas clouds). These will be important for considerations of star formation (see § IV). On the other hand, large-scale shock waves (with a typical scale of a few kpc) have been considered by Fujimoto (1966) in the flow of gas through a model spiral arm. Although Fujimoto's calculations represent an important first step in the determination of the nonlinear dynamics of the gaseous component of the galactic disk, they cannot account for a two-armed galactic shock pattern. Instead, they exhibit a multiarmed spiral potential that possesses from four to about ten spiral arms.[1] Of especial interest in the present investigation is the physical picture of a *two-armed* grand design of spiral structure that is characteristic of the majority of normal spiral disk-shaped galaxies.

We might expect self-sustained density waves in the galactic disk to grow and develop in the course of time into disturbances with a shocklike nature.[2] Thus, the self-sustained density waves obtained by Lin and Shu would be expected to develop into shocks with a regular two-armed grand design of spiral structure over the disk. It is, however, not obvious a priori that two periodically located spiral shock waves present throughout the galactic disk would be compatible with the general nature of a stationary gas flow about the disk. This compatibility is just what must be confirmed.

II. DYNAMICS OF A DISK-SHAPED GALAXY

The dynamics of the stellar component of the galactic disk is primarily governed by the inertial force associated with the rotation of the disk and the smoothed gravitational

[1] A comparison of the basic differences between Fujimoto's work and the present investigation is given in § V.

[2] The process of shock development in the course of time will be considered in another paper.

force of the system as a whole. When we consider the dynamics of the gaseous component, we should also include the gaseous "pressure" associated with turbulence in the interstellar medium[3] and the hydromagnetic forces due to magnetic fields embedded in the gas. Furthermore, we should also include the effects due to cosmic rays, supernova explosions, and stellar radiation, which are the primary sources of turbulent energy for the gas, and the effect of dissipation of turbulence by collisions of gas clouds, which is the primary sink of turbulent energy for the gas. In our picture, which provides a first approximation to the total nonlinear galactic picture, turbulence, together with the inertial and gravitational effects, is included. Each gas streamtube is visualized to possess a uniform mean turbulent dispersion speed. With this implicit energy balance, the gas flow along each streamtube is isothermal at a uniform mean equivalent turbulent temperature.

Yuan (1969) has carried out calculations for the imposition of a magnetic field on the large-scale galactic gas flow in the framework of a linear theory and has shown that for a magnetic field on the order of 5×10^{-6} gauss, the streamlines do not deviate greatly from the streamlines of the gas flow without the presence of the magnetic field. A magnetic field no larger than 5×10^{-6} gauss may be expected to influence only secondary effects in the dynamics of the gas in the nonlinear theory as well as in the linear theory, and therefore such a magnetic field will not be considered further in the large-scale shock investigations.

Since the major proportion of gas and stars are evidently located in a layer whose thickness is about $\frac{1}{50}$ to $\frac{1}{100}$ the diameter of the galactic disk, the disk may be imagined as a very thin sheet. We therefore consider mean values of the physical variables integrated over the sheet thickness. In terms of these mean variables, the dynamics of the disk is two-dimensional in nature, with the forcing mechanisms and the responses confined entirely within the sheet. Although there are really two separate components of the disk, gaseous and stellar, we shall be primarily concerned with the determination of the response of the gaseous component to an imposed background spiral gravitational field which may be attributed to the more massive stellar component that forms a spiral pattern.[4]

a) Dynamical Equations Governing the Gaseous Disk

The fundamental equations of motion for gas flow about a circular disk, where u_ϖ and u_θ represent the velocity components in the ϖ and θ directions, respectively (see Fig. 1), may be written by an observer in an inertial frame of reference as:

$$\frac{\partial \sigma}{\partial t} + \frac{1}{\varpi}\frac{\partial(\sigma u_\varpi \varpi)}{\partial \varpi} + \frac{1}{\varpi}\frac{\partial(\sigma u_\theta)}{\partial \theta} = 0\,, \tag{1}$$

$$\frac{\partial u_\varpi}{\partial t} + u_\varpi \frac{\partial u_\varpi}{\partial \varpi} + \frac{u_\theta}{\varpi}\frac{\partial u_\varpi}{\partial \theta} - \frac{u_\theta^2}{\varpi} = -\frac{a^2}{\sigma}\frac{\partial \sigma}{\partial \varpi} - \frac{\partial \mathfrak{U}}{\partial \varpi}\,, \tag{2}$$

$$\frac{\partial u_\theta}{\partial t} + u_\varpi \frac{\partial u_\theta}{\partial \varpi} + \frac{u_\theta}{\varpi}\frac{\partial u_\theta}{\partial \theta} + \frac{u_\varpi u_\theta}{\varpi} = -\frac{a^2}{\sigma \varpi}\frac{\partial \sigma}{\partial \theta} - \frac{1}{\varpi}\frac{\partial \mathfrak{U}}{\partial \theta}\,, \tag{3}$$

where t denotes the time, $\sigma(\varpi,\theta,t)$ is the gas density of the galactic disk, a is the mean turbulent dispersion speed of the gas, and $\mathfrak{U}(\varpi,\theta,t)$ is the total gravitational potential.

[3] If the interstellar medium is indeed a nonquiescent one as shown by observations, then the pressure due to turbulence must be larger than the kinetic pressure.

[4] We shall see later that the imposed field may actually be regarded as the *resultant* gravitational field of gas, young stars, and moderately old stars.

b) Base State of Motion

We take for the base state of motion an equilibrium state of purely circular gas flow where the total smoothed central gravitational force field is exactly balanced by the inertial force associated with the rotation of the disk as a whole. The gas density of the base state is taken as $\sigma_0(\varpi)$, and the smoothed gravitational potential field is denoted by $\mathfrak{U}_0(\varpi)$. For purely circular flow, we have $u_\varpi = 0$ and $u_\theta = \Omega(\varpi)\varpi$; and the relation for the balance of radial forces may be written as:

$$\Omega^2(\varpi)\varpi = \frac{d\mathfrak{U}_0(\varpi)}{d\varpi} . \tag{4}$$

For our own Milky Way system the base state of motion that satisfies the above balance of radial forces is described by the Schmidt model (see Schmidt 1965).

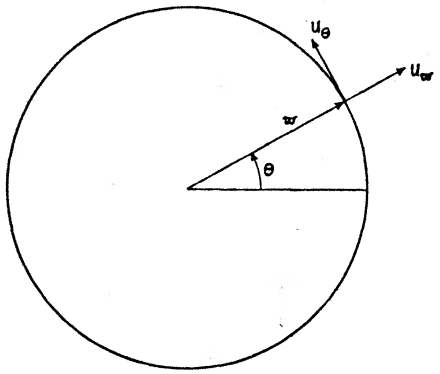

FIG. 1

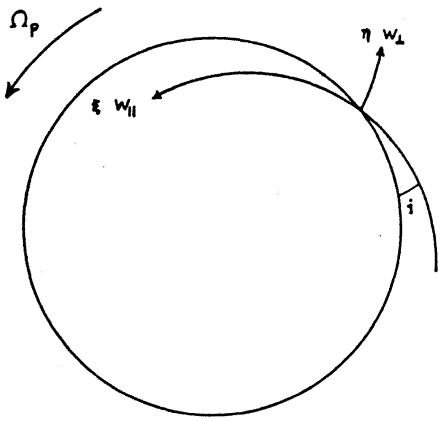

FIG. 2

FIG. 1.—The (ϖ,θ)-coordinate system for the galactic disk.

FIG. 2.—The (ξ,η)-coordinate system, which rotates with the angular speed Ω_p of the spiral pattern. ξ and η run parallel and perpendicular to spiral equipotential curves marking out the spiral arms in the galactic disk, i is the angle of inclination of the spiral arm to the circumferential direction.

c) Perturbed State

Since we are dealing with a galactic system where the gravitational field consists of a two-armed spiral field superposed on the Schmidt model, we may divide the total gravitational potential into two portions:

$$\mathfrak{U}(\varpi,\theta,t) = \mathfrak{U}_0(\varpi) + \mathfrak{U}_1(\varpi,\theta,t) ,$$

where $\mathfrak{U}_0(\varpi)$ is the smoothed gravitational potential corresponding to the Schmidt model for the Milky Way system, and $\mathfrak{U}_1(\varpi,\theta,t)$ is the spiral gravitational potential corresponding to the two-armed spiral pattern. We take $\mathfrak{U}_1(\varpi,\theta,t)$ of the form:

$$\mathfrak{U}_1(\varpi,\theta,t) = A(\varpi,\theta)\cos\left\{2\Omega_p t - 2\left[\frac{1}{\tan i}\ln\left(\frac{\varpi}{\varpi_0}\right) + \theta\right] - \phi\right\} , \tag{5}$$

where $A(\varpi,\theta)$ is a slowly varying function of ϖ and θ, and where ϕ is a constant phase angle.

In a similar manner, each physical variable may be divided into a portion correspond-

ing to the axisymmetric equilibrium state of the Schmidt model plus a portion corresponding to the perturbation due to the spiral gravitational field:

$$\sigma(\varpi,\theta,t) = \sigma_0(\varpi) + \sigma_1(\varpi,\theta,t) ,$$

$$u_\varpi(\varpi,\theta,t) = 0 + u_{\varpi 1}(\varpi,\theta,t) , \quad u_\theta(\varpi,\theta,t) = \Omega(\varpi)\varpi + u_{\theta 1}(\varpi,\theta,t) .$$

Since the spiral pattern rotates as a rigid structure, it would be convenient to describe the gas flow from a vantage point on a rotating coordinate system fixed with respect to the spiral pattern which rotates with angular velocity Ω_p. Furthermore, the form of the spiral potential, $U_1(\varpi,\theta,t)$, indicates that a convenient set of coordinates to be used for describing the gas flow is the set of coordinates fixed in the Ω_p-rotating system that are parallel and perpendicular to the spiral equipotential curves (see Fig. 2). These coordinates may be written as follows:

$$\begin{aligned} \eta &= \ln(\varpi/\varpi_0)\cos i + (\theta - \Omega_p t)\sin i , \\ \xi &= -\ln(\varpi/\varpi_0)\sin i + (\theta - \Omega_p t)\cos i . \end{aligned} \tag{6}$$

The velocity components along these coordinates may be written as:

$$\begin{aligned} w_{\perp 0} &= (\Omega - \Omega_p)\varpi \sin i , & w_{\parallel 0} &= (\Omega - \Omega_p)\varpi \cos i , \\ w_\perp &= u_{\varpi 1}\cos i + u_{\theta 1}\sin i , & w_\parallel &= -u_{\varpi 1}\sin i + u_{\theta 1}\cos i . \end{aligned} \tag{7}$$

d) Asymptotic Theory

Since the imposed spiral potential is oscillatory as cosine in η and only slowly varying in ξ, we expect the physical-perturbation solution of interest to be likewise oscillatory in η and only slowly varying in ξ. Indeed, this is precisely the case in the linear density-wave theory where all perturbation quantities are of the general form

$$P(\eta,\xi)\exp[iQ(\eta)] ,$$

where $P(\eta,\xi)$ is slowly varying in η and ξ, and where $Q(\eta) = -(2/\sin i)\eta$. Moreover, we are interested in stationary, or at least quasi-stationary, gas flow. Therefore, we look for solutions for which the induced perturbation quantities are weakly dependent on ξ and t in comparison with their dependence on η. We exhibit this behavior by introducing the small parameters δ_1 and δ_2 and by regarding the physical variables as

$$\sigma_1(\eta,\delta_1\xi,\delta_2 t) , \quad w_\perp(\eta,\delta_1\xi,\delta_2 t) , \quad w_\parallel(\eta,\delta_1\xi,\delta_2 t) . \tag{8}$$

We therefore make the asymptotic approximation in which the perturbation quantities to first order vary only along the direction normal to the contours of constant phase.[5]

To first order in the asymptotic analysis, the asymptotic equations of gas flow may be written as:

$$(w_{\perp 0} + w_\perp)\frac{\partial \sigma_1}{\partial \eta} + (\sigma_0 + \sigma_1)\frac{\partial w_\perp}{\partial \eta} + \left(\sigma_0 + \sigma_1 + \varpi\frac{d\sigma_0}{d\varpi}\right)\chi_1 + O(\delta_1,\delta_2) = 0 , \tag{9}$$

$$(w_{\perp 0} + w_\perp)\frac{\partial w_\perp}{\partial \eta} - 2\Omega\varpi w_\parallel + \frac{a^2}{\sigma_0 + \sigma_1}\frac{\partial \sigma_1}{\partial \eta} + \frac{\partial U_1}{\partial \eta} + \chi_2 + O(\delta_1,\delta_2) = 0 , \tag{10}$$

$$(w_{\perp 0} + w_\perp)\frac{\partial w_\parallel}{\partial \eta} + \left(\frac{K^2}{2\Omega}\right)\varpi w_\perp + \chi_3 + O(\delta_1,\delta_2) = 0 , \tag{11}$$

[5] This asymptotic approximation has been confirmed by the numerical calculations; in the case, $\tan i = \frac{1}{7}$, the variation in the perturbation quantities along the equipotential contours is $O(\frac{1}{8})$ of their variation normal to these contours.

where

$$\left(\frac{K^2}{2\Omega}\right) = 2\Omega\left(1 + \frac{\varpi(d\Omega/d\varpi)}{2\Omega}\cos^2 i\right), \tag{12}$$

$$\chi_1 = (w_\perp \cos i - w_\parallel \sin i), \tag{13}$$

$$\chi_2 = \varpi^2\frac{d\Omega}{d\varpi}\sin i(w_\perp \cos i - w_\parallel \sin i) - w_\parallel(w_\perp \sin i + w_\parallel \cos i) + \frac{a^2\varpi \cos i}{\sigma_0 + \sigma_1}\frac{d\sigma_0}{d\varpi}, \tag{14}$$

$$\chi_3 = \varpi^2\frac{d\Omega}{d\varpi}\cos i(-w_\parallel \sin i) + w_\perp(w_\perp \sin i + w_\parallel \cos i) - \frac{a^2\varpi \sin i}{\sigma_0 + \sigma_1}\frac{d\sigma_0}{d\varpi}, \tag{15}$$

and

$$\mathfrak{U}_1 = A\cos\left(-\frac{2}{\sin i}\eta - \phi\right). \tag{16}$$

Although the terms containing χ_1, χ_2, and χ_3 in equations (9), (10), and (11) are all of secondary importance, they will be retained in the numerical calculations.

Eliminating σ_1 between equations (9) and (10) and defining the perturbation force as

$$f = -\frac{1}{\varpi}\frac{\partial \mathfrak{U}_1}{\partial \eta}, \tag{17}$$

we can rewrite equations (10) and (11) in the form:

$$\frac{\partial w_\perp}{\partial \eta} = -\frac{(w_{\perp 0} + w_\perp)(2\Omega\varpi w_\parallel + \varpi f - \chi_2) + a^2\{1 + [\varpi/(\sigma_0 + \sigma_1)]d\sigma_0/d\varpi\}\chi_1}{a^2 - (w_{\perp 0} + w_\perp)^2}, \tag{18}$$

$$\frac{\partial w_\parallel}{\partial \eta} = -\frac{(K^2/2\Omega)\varpi w_\perp + \chi_3}{w_{\perp 0} + w_\perp}, \tag{19}$$

where

$$f = F\varpi\Omega^2 \sin\left(\frac{2}{\sin i}\eta + \phi\right), \qquad F = \frac{2A/(\varpi \sin i)}{\varpi\Omega^2}. \tag{20}$$

Here F is the amplitude of the perturbation force as a fraction of the mean axisymmetric gravitational field. Equations (18) and (19) are two asymptotic equations to be solved for the two dependent variables $w_\perp$ and $w_\parallel$. Once we have $w_\perp(\eta)$ and $w_\parallel(\eta)$, we can determine $\sigma_1(\eta)$ by solving the equation

$$(w_{\perp 0} + w_\perp)\frac{\partial \sigma_1}{\partial \eta} + (\sigma_0 + \sigma_1)\frac{\partial w_\perp}{\partial \eta} + \left(\sigma_0 + \sigma_1 + \varpi\frac{d\sigma_0}{d\varpi}\right)\chi_1 = 0, \tag{21}$$

and we can determine our position about the disk (specified by ξ) by solving the equation

$$\frac{\partial \xi}{\partial \eta} = \frac{w_{\parallel 0} + w_\parallel}{w_{\perp 0} + w_\perp}. \tag{22}$$

Solution of the system of equations (18), (19), (21), and (22), determines a gas streamtube as well as the gas flow at every point along the streamtube.

e) Gas Streamtube through Two Periodically Located Shocks

We are primarily interested in a particular type of solution of the nonlinear gas flow equations that satisfies three requirements:

1. It should permit the gas to pass through two periodically located shock waves which lie coincident with spiral equipotential curves in the disk.

2. It should describe the gas flow along a narrow, nearly concentric streamtube band about the galactic center, and the streamtube should repeat itself through every half-revolution of the gas flow about the disk.

3. It should insure closure of the gas streamtube so that no net radial transfer of mass, momentum, or energy takes place across the streamtube.

This solution is one for gas flow in a closed, nearly concentric, and twice-periodic *streamtube* band through *two* periodically located *shock* waves and is hereinafter referred to as an STS solution.

There are five basic independent parameters that govern the nature of the STS solution:

i, angle of inclination of a spiral arm to the circumferential direction;
Ω_p, angular speed of the spiral pattern;
F, amplitude of the spiral gravitational field taken as a fixed fraction of the smoothed axisymmetric gravitational field;
ϖ, average radius of the streamtube;
$a(\varpi)$, mean turbulent dispersion speed of the gas along the streamtube.

Once these five parameters are specified and requirements (1), (2), and (3) are satisfied, the shock location with respect to the background spiral arm is automatically determined. Figure 3 provides a plot in $(W_\perp[=w_{\perp 0}+w_\perp], W_\parallel[=w_{\parallel 0}+w_\parallel], \theta_{\Omega_p})$-space of a typical STS solution for the set of parameters: $\tan i = \frac{1}{7}$, $\Omega_p = 12.5$ km sec^{-1} kpc^{-1}, $F = 5$ percent, $\varpi = 10$ kpc, and $a = 10$ km sec^{-1}. The motion of the gas described by this typical STS solution may be visualized in simplified terms as the nonlinear counterpart of epicyclic motion, as modified by gaseous "pressure."

III. RESULTS

a) *Stationary Two-Armed Spiral Shock Pattern*

Numerical calculations for regions with radii between 3–4 and 12 kpc in the Schmidt model confirm the compatibility of two periodically located shocks lying along and within the imposed two-armed background spiral pattern. The composite gas flow picture over the whole galactic disk is made up of a family of STS solutions and describes gas flow in closed, nearly concentric, and twice-periodic streamtube bands that pass through a *two-armed spiral shock* pattern (this composite picture of gas flow is hereinafter referred to as the TASS picture). Figure 4 illustrates the position of the TASS pattern inside the background spiral pattern. The background pattern may be regarded as the composite pattern of all the moderately old stars of ages greater than perhaps 30 million years and therefore does not stand out in observational studies. Streamlines which turn sharply at each shock are sketched for several typical radii. Figure 5 illustrates the behavior of the gas density, $\sigma'(=[\sigma_0+\sigma_1]/\sigma_0)$ and the velocity components, $W_\perp(=w_{\perp 0}+w_\perp)$ and $W_\parallel(=w_{\parallel 0}+w_\parallel)$, along a typical streamtube in the TASS picture. It is interesting to note that the shock lies just on the inner side of the background spiral arm of trailing type.

Investigation of a number of typical gas clouds (see Spitzer 1968) has shown that the large clouds may not be far from the critical condition where gravitational collapse becomes possible. On the basis of this investigation and the above results, it is now suggested that galactic shock waves may very well form the triggering mechanism for the gravitational collapse of gas clouds, leading to star formation. Since newly born stars give rise to H II regions, galactic shocks may be visualized as the necessary forerunners of the prominent H II regions as well as the newly born stars. Before reaching the shock, some of the large clouds and cloud complexes may be on the verge of gravitational col-

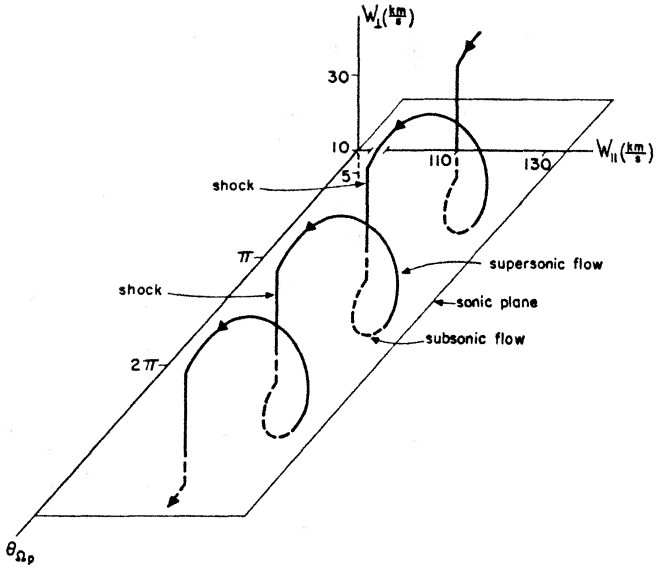

FIG. 3.—A Typical STS Solution. In passing through two cycles of the STS solution, the gas completes one revolution about the two-armed spiral pattern in the galactic disk. Gas enters the shock at a supersonic velocity normal to the shock of about 31 km sec^{-1} and leaves the shock at a subsonic velocity normal to the shock of about 3.2 km sec^{-1}. The density contrast across the shock is about 9.6.

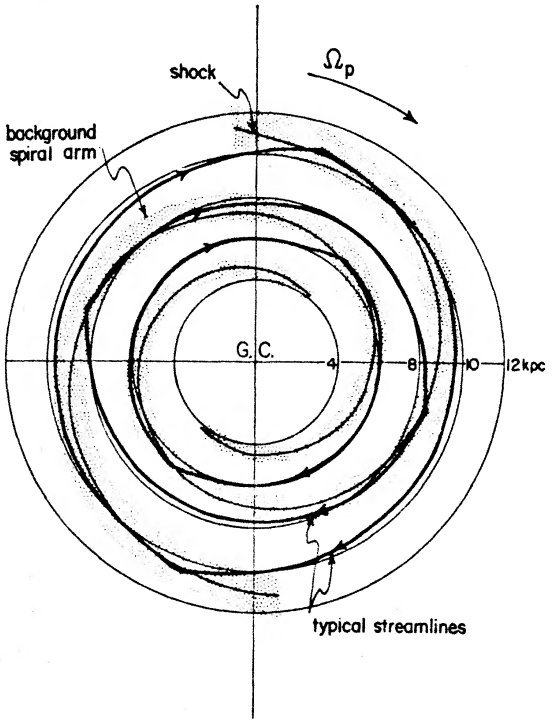

FIG. 4.—Shock and background spiral pattern in the Galaxy. The shock occurs slightly on the inner side of the background spiral arm of trailing type. In the TASS picture each streamline appears as a sharp-pointed oval with a sharp turning point at each shock.

lapse. A sudden compression of the clouds in the shock to perhaps 8 or 10 times their original density could conceivably trigger the gravitational collapse of some of the largest gas clouds. As the gas leaves the shock region, it is rather quickly decompressed, and star formation ceases. In Figure 6 the region of most prominent star formation is superposed on the distribution of gas density along a typical streamtube of the TASS picture. The region extending from the shock to the point where the gas density drops below its average value of unity corresponds to the observable gaseous spiral arm. If

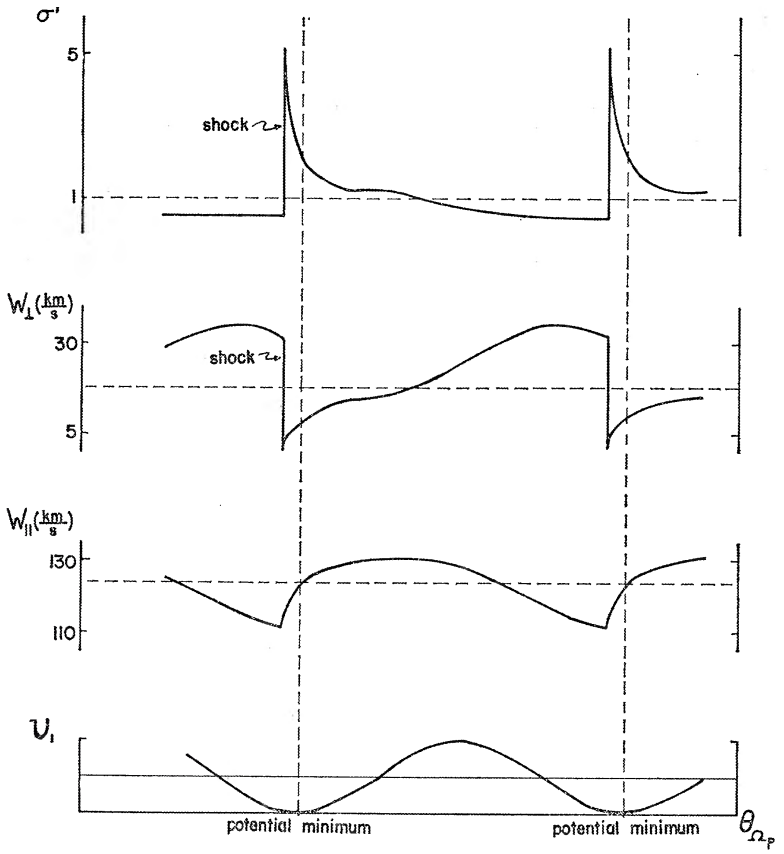

FIG. 5.—A typical solution in the TASS picture. This solution is the STS solution sketched in ($W_\perp$, $W_\parallel$, θ_{Ω_p})-space in Fig. 3. With a pattern speed, Ω_p, of 12.5 km sec^{-1} kpc^{-1}, and an angle of inclination i such that $\tan i = \frac{1}{7}$, this STS solution in the TASS picture describes the gas flow at a radius of 10 kpc under a spiral field of 5 percent of the axisymmetric field and with a mean gaseous dispersion speed of 10 km sec^{-1}.

an upper bound of 30 million years is assumed for the process of formation and evolution of relatively massive stars initiated at the shock, the possible locations of the regions of newly born luminous stars and H II regions lie on the inner side of the observable gaseous spiral arm of H I, extending from the sharp H I peak at the shock on the inner edge to approximately the center of the arm.[6]

We can now visualize how the Galaxy may appear with shocks present. When observations of the galactic disk are made, the background distribution of moderately old stars making up the imposed two-armed spiral pattern is not seen. Basically, what we do see are: (1) the observable gaseous spiral arms of H I, and (2) the newly born luminous stars and brilliant H II regions. Figure 7 illustrates this observable physical picture ac-

[6] In any given case, there may be only a very narrow region that is prominent, because the gaseous clouds (before reaching the shock) might be predominantly of one typical size and density.

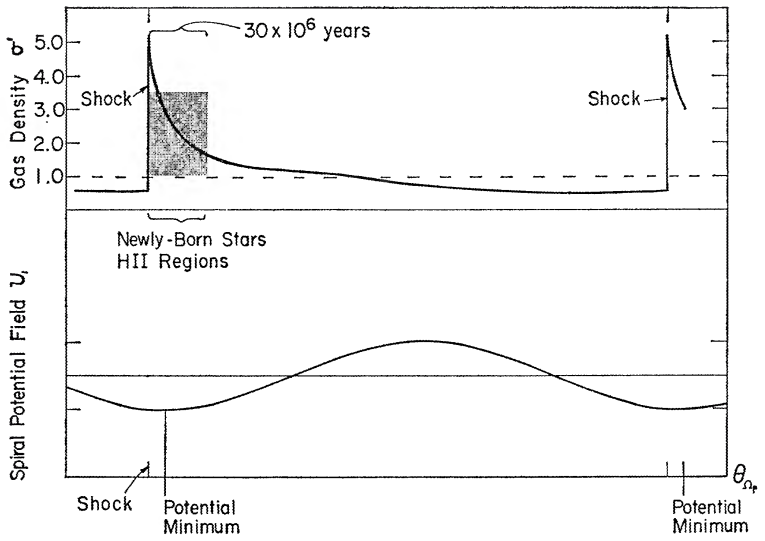

FIG. 6.—Gas-density distribution along a typical streamtube in the TASS picture. The potential minimum corresponds to the density maximum and the center of the background spiral arm. Although the H I is especially prominent in the sharp peak adjacent to the shock, the H I arm actually extends from the shock to the location where the gas density drops below its average value of unity. Depending on the time necessary for triggering the formation of stars at the shock from gas clouds of various sizes, the regions of the newly born stars and the H II regions may vary in width from quite narrow to somewhat broad. Allowing a typical time of 30 million years for the formation and evolution of the relatively massive stars, the possible locations of the regions of the newly born stars and the H II regions lie just outside the sharp H I peak on the inner side of the overall H I arm.

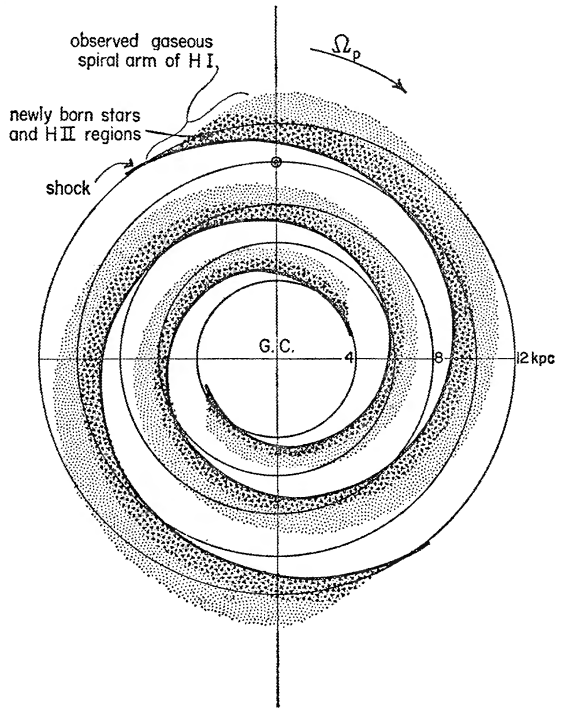

FIG. 7.—Spiral pattern in the Galaxy: the observable picture. The location of the shock and the sharp H I peak and the possible locations of the regions of newly born luminous stars and the H II regions lie on the inner side of the observable gaseous spiral arm of H I (of trailing type).

cording to the shock predictions. A shock, together with a sharp H I peak, occurs on the inner edge of the observable gaseous spiral pattern of H I. On the inside of this observable spiral pattern (but just outside the shock and the sharp H I peak) lie the regions of newly born stars and the H II regions. This is an important feature of the shock theory that Westerhout (1968) has in fact found in observational studies of the Milky Way system.

We shall refer to a shock of the TASS pattern in two different ways. While it is sometimes convenient to consider the *shock strength* which is equivalent to the density contrast across the shock (i.e., $\sigma(2)/\sigma(1)$), at other times it is convenient to consider the *effective gas compression* along a streamtube, which is taken as the ratio of the maximum gas density to the average gas density (i.e., $\sigma(2)/\sigma_0$). With the spiral field having a magnitude of about 5 per cent of the axisymmetric field and with a uniform mean turbulent dispersion speed of about 10 km sec^{-1} over the disk, the *effective gas compression* of the TASS pattern rises monotonically with decreasing radius from about 5 in the 10-kpc region to 6–7 in the neighborhood of 3–4 kpc. Under the same field and the same uniform dispersion speed, the shock strength shows a slight dip to about 6 in the region of 6–7 kpc and rises on either side to about 10 in the 10-kpc region and to 7–9 in the neighborhood of 3–4 kpc.[7] On the other hand, if the dispersion speed were to decrease with decreasing radius, the effective gas compression and the shock strength would exhibit much larger values in the neighborhood of 3–4 kpc. For example, with a dispersion speed of about 8 km sec^{-1} in the neighborhood of 3–4 kpc, the effective gas compression would be 7–10 and the shock strength would be 8–12. Since it is the maximum value of gas density that suggests the actual degree of gas-cloud compression and possibly the relative amounts of star formation and H II concentrations at various radii, it is likely that the effective gas compression provides a better indication of star formation than does the shock strength. It is interesting to note that the effective gas compression becomes nearly uniform over the TASS pattern when the mean gaseous dispersion speed increases slightly with decreasing radius, e.g., from 10 km sec^{-1} at 10 kpc to about 11–12 km sec^{-1} at 3–4 kpc. In this situation even without a rise in effective gas compression, the effect of increasing gaseous turbulent dispersion speed (with the accompanying effect of increasing density variation in gaseous clouds) toward the inner regions may contribute to a relative rise in star formation and H II concentration in the 4-kpc neighborhood. In each of these cases this feature of enhanced star formation and H II concentration toward the inner regions of the galactic disk, as a result either of increased effective gas compression or of increased density contrast in the large clouds, shows general agreement with observational evidence of the mean H II distribution plotted with respect to radius over the galactic disk between 3–4 kpc and 10 kpc (see Kerr and Westerhout 1965; Kerr *et al.* 1968).

b) Outer Bound Cutoff of the TASS Pattern in the Schmidt Model

Numerical calculations have been carried out over the disk out to the outer bound of 12–13 kpc where the TASS pattern terminates. According to the shock theory, outside a radius of 12–13 kpc a multiarmed spiral shock pattern is possible only if the number of arms exceeds two. For a larger spiral field, the outer cutoff of the TASS pattern would lie at a larger radius in the disk. For example, the outer cutoff for a 7.5 per cent field would lie at 13–14 kpc. Observational evidence for an outer cutoff of the TASS pattern in many Sc-type galaxies appears in the observational studies of M. S. Roberts (1967) which show that the optical arms lie significantly interior to the H I peak.

c) The Limit of Weak Shock Strength and Weak Spiral Gravitational Field

The phase of the fundamental component of gas density distribution in an STS solution making up a portion of the TASS picture approaches the phase of the linear density

[7] With a smaller mean gaseous turbulent dispersion speed and/or a larger field strength, a TASS pattern containing even larger effective gas compression and shock strength could be maintained.

solution as the field strength decreases (see Roberts 1968*b*). Suppose we now consider an important related limiting process, namely, whether an STS solution and a TASS pattern can persist in the limit of zero field. It would be interesting to determine whether a limit for decreasing field (at constant dispersion speed of the gas) does exist below which no two-shock gas-streamtube solution is possible. Indeed, this is found to be the case. According to the numerical calculations, in order to retain the STS solution as the field decreases, the shock phase Φ_s must also decrease. Projections of a typical STS solution in $w'_\perp$ $(= w_\perp/2\Omega\varpi)$ and $w'_\parallel$ $(= w_\parallel/2\Omega\varpi)$ space for the set of parameters $\tan i = \frac{1}{7}$, $(K/2\Omega)^2 = 0.4$, $w'_{\perp 0} = 0.049$, and a' $(= a/2\Omega\varpi) = 0.034$, and for several values of the field strength, $F = 7.5$, 5, 2, 1.28, 1.16, 1.04, and 0.8 percent, are sketched in Figure 8. The shock strength and the Mach number, M_1 (supersonic), decrease as the strength of the field decreases. Table 1 provides the various shock strengths and Mach numbers (supersonic) under these respective field strengths. For the above set of values of the parameters, a limit is found for the field strength below which no STS solution is possible. This limit of *finite* shock strength is:

$$\frac{\sigma(2)}{\sigma(1)} = 1.4\,, \qquad M_1 = 1.2\,,$$

and occurs for a field of about 1.04 per cent of the axisymmetric field. In general, for every other set of values of the parameters, similar lower bounds exist on the field and the shock strength of the associated STS solution. In fact, for every radius between 3–4 kpc and 12 kpc in the galactic disk, there is a positive lower bound on shock strength for every STS solution and a positive lower bound for the spiral field which is necessary to support the STS solution.

d) Free Spiral Mode

Something exceptional occurs in the 3-kpc neighborhood of the galactic disk. Indeed, for an STS solution at a radius of about 3 kpc the lower bound for the field is *zero* while the corresponding lower bound for the shock strength is still *finite*. Therefore, it is possible for an *STS free mode* to exist in the 3-kpc neighborhood of the Schmidt model, whereas such an STS free mode is not possible over any other portion of the disk outside 3 kpc.

Since no background spiral pattern is necessary for the support of the gaseous STS free mode, its leading or trailing nature is not necessarily predetermined by any imposed background pattern. Therefore, an STS free mode of both leading and trailing types is possible. Figures 9 and 10 illustrate the physical pictures of the possible STS free modes of trailing and leading type. The radial velocity along each streamtube is large and positive over two short arcs lying directly across the galactic center from one another. In the trailing case, the least dense regions move radially outward, while the *most* dense regions move radially *inward*. On the other hand, in the leading case, the *most* dense regions move radially *outward*, while the least dense regions move radially inward. The picture for an STS free mode of leading type therefore better helps to account for the "3-kpc arm" in the Galaxy which is apparently undergoing rapid radial expansion away from the galactic center toward the solar neighborhood. Conversely, if the "3-kpc arm" of observational studies were actually located on the far side of the galactic center from the solar neighborhood, the STS free mode of trailing type would better help to account for its rapid inward motion toward the galactic center and toward the solar neighborhood.

Even larger excitation and response of the gas flow in the 3-kpc neighborhood is possible in the presence of an imposed spiral background field. Numerical calculations have been carried out for STS solutions in the 3-kpc neighborhood under fields with magnitudes of 5, 10, and 15 percent of the axisymmetric field. An effective gas compres-

sion of 65, a maximum radial velocity of 40 km sec^{-1}, and a shock strength of 180 are typical estimates for an STS solution under a 15 percent field.

e) Physical Picture for a TASS Pattern in a Spiral Galaxy of Leading Type

Figure 11 illustrates the nature of a typical STS solution in the TASS patterns of spiral galaxies of leading and trailing types. The symmetry of the two cases is apparent, as expected. The calculations for radii between 3–4 and 12 kpc in the Schmidt model have confirmed that a TASS pattern of leading type is indeed compatible with the gen-

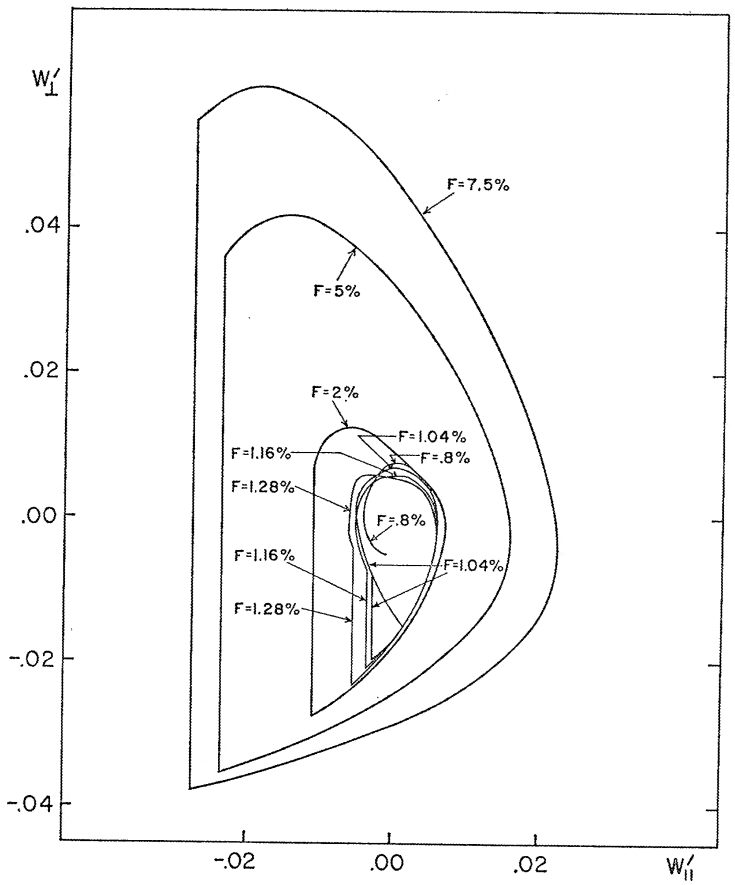

FIG. 8.—Lower bound on shock strength and background spiral field for a typical STS solution. If the background spiral gravitational field is too small, no STS solution can be sustained.

TABLE 1

LIMIT OF DECREASING FIELD AND SHOCK STRENGTH OF AN STS SOLUTION

$F(\%)$	$\sigma(2)/\sigma(1)$	M_1
7.5.....	9.2	3.0
5.0.....	6.2	2.5
2.0.....	2.4	1.6
1.28.....	1.9	1.4
1.16.....	1.5	1.22
1.04.....	1.4	1.2

eral nature of a stationary gas flow about the galactic disk of leading type. In the TASS picture of leading type, the shock lies just on the outer side of the imposed background spiral arm.

Since the gas flow across a shock of leading type has an inward radial motion, the region of largest gaseous concentration (i.e., the sharp H I peak) occurs just inside the shock. Therefore, the shock in a spiral galaxy of leading type lies on the outer edge of the observable gaseous spiral arm of H I. In this situation, the possible locations of the regions of newly born luminous stars and the H II regions lie on the outer side of the

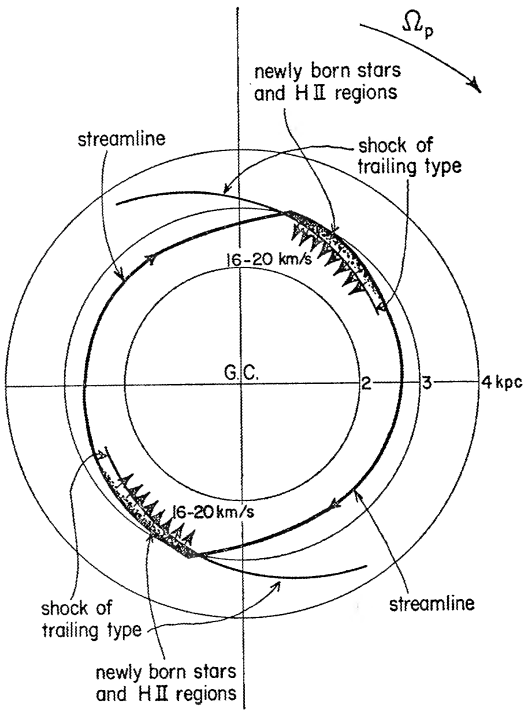

FIG. 9

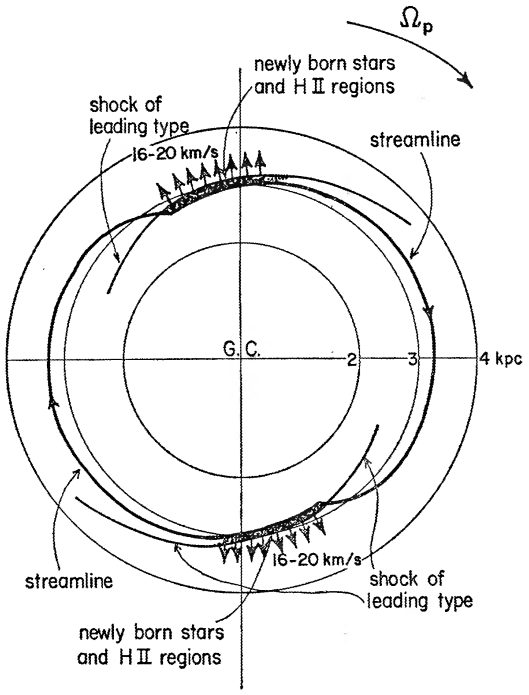

FIG. 10

FIG. 9.—The free mode of trailing type in the 3-kpc neighborhood. No background spiral gravitational field is necessary to support the two-shock picture in the 3-kpc neighborhood. The regions of newly born stars, the H II regions, and the region of largest H I concentration along the streamtube possess an inward radial component of velocity of about 16–20 km sec^{-1}.

FIG. 10.—The free mode of leading type in the 3-kpc neighborhood. No background spiral gravitational field is necessary to support the two-shock picture in the 3-kpc neighborhood. The regions of newly born stars, the H II regions, and the region of largest H I concentration along the streamtube possess an outward radial component of velocity of about 16–20 km sec^{-1}.

observable gaseous spiral arm of H I, extending from the sharp H I peak at the shock on the outer edge to approximately the center of the arm. By observational studies of spiral galaxies, it may therefore be possible to distinguish spiral galaxies as leading- or trailing-type systems and to determine their sense of rotation as well, according to the location of the regions of most prominent star formation and the most brilliant H II regions on the outer or inner edge of the observable gaseous spiral arm of H I.

IV. STAR FORMATION ALONG SPIRAL ARMS

The process of gravitational collapse of an isolated system similar to a cloud of our model but containing no turbulence is well known (see Chandrasekhar 1942; Ebert

1955; Spitzer 1968). We now consider a simple gas-cloud model consisting of an isothermal sphere of gas in thermal equilibrium with a surrounding medium of rarefied gas, all in turbulent motion. Although internal turbulence enhances the cloud with an equivalent temperature and pressure that tend to prevent self-gravitational collapse, it also provides the cloud with internal fragmentation which influences the formation of many protostars inside the cloud once the collapse process has been initiated. For a given cloud (in our nonquiescent model) of mass M at a kinetic temperature T, and with an internal

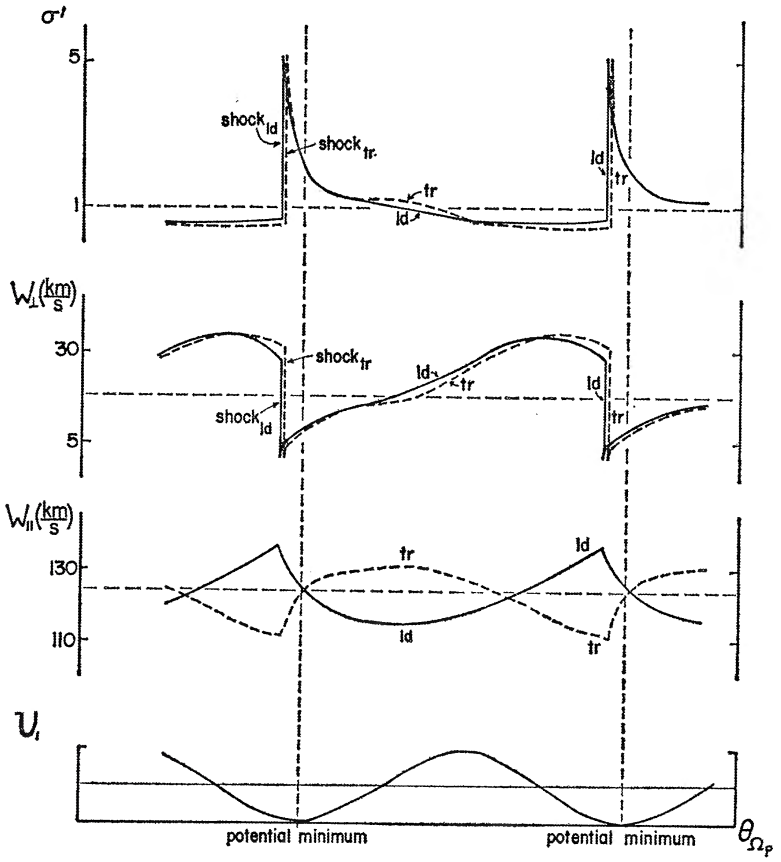

FIG. 11.—A typical STS solution in the TASS pictures of spiral galaxies of leading (ld) and trailing (tr) type. Whereas in the trailing case the gas flows across the spiral arm from the inner to the outer side, in the leading case the gas flows across the spiral arm from the outer to the inner side. The symmetry of the two STS solutions is very striking.

rms turbulent dispersion speed, $(\overline{v^2})^{1/2}$, corresponding to an effective turbulent temperature, there is a maximum surface pressure, $p_{\max}$, dependent on the total equivalent temperature (partly kinetic and partly due to turbulence) which the isothermal cloud can withstand. If the surface pressure were increased to a value exceeding $p_{\max}$ during the passage of the cloud through a large-scale shock, no equilibrium configuration would be possible, and the cloud would be forced into rapid gravitational collapse.

a) Typical Large Galactic Gas Clouds

Spitzer (1968) discusses a number of large galactic gas clouds taken from observational studies. Table 2 lists some of these typical large clouds. The kinetic temperatures of clouds of these types have been generally estimated to lie within the range of 60°–120° K. A value of 100° K might be a reasonable estimate for the mean kinetic tempera-

ture characteristic of this group of clouds as a whole. Estimates have also been made of the state of turbulence in galactic gas clouds, and it appears that an rms turbulent dispersion speed between 0.5 and 2 km sec^{-1} would provide a typical estimate of the state of turbulence (see Clark, Radhakrishnan, and Wilson 1962; Barrett, Meeks, and Weinreb 1964).

b) Necessity for a Large-Scale Galactic Shock

A simple criterion for determining those clouds which are beyond their verge of gravitational collapse may be written in terms of $\langle n \rangle$, M, and T_{equiv} as

$$\langle n \rangle_{\text{crit}} = 10^3 \frac{(T_{\text{equiv}})^3}{(M/M_\odot)^2} . \tag{23}$$

Those clouds with mean density $\langle n \rangle > \langle n \rangle_{\text{crit}}$ are in the collapsing stage, whereas those clouds with mean density $\langle n \rangle < \langle n \rangle_{\text{crit}}$ are not so compact as to lie beyond their verge of gravitational collapse. For example, typical clouds of mass $M = 10^4\ M_\odot$ with equivalent temperature $T_{\text{equiv}} = 300°$ K require a critical density of about 270 H cm^{-3} to lie on their verge of collapse under the influence of just their self-gravitation alone without the influence of external compressive effects. In reality, large clouds observed in the interstellar medium generally have densities nowhere near this large a value. It is

TABLE 2

TYPICAL LARGE GALACTIC GAS CLOUDS

Cloud Type	$M/M_\odot$	R (pc)	$\langle n \rangle$ (H cm^{-3})
"Large" cloud.....	1.8×10^4	20	20
A large cloud.....	10^4	17	20
"Typical large" cloud	7×10^3	15	20

therefore rather difficult to explain the present-day formation of young stellar associations on the basis of the self-gravitation of gas clouds alone without some other triggering mechanism.

On the other hand, suppose a large-scale galactic shock wave exists in the galactic disk. Under the influence of a shock with 8:1 strength typical of the TASS pattern, a simple criterion for determining those clouds which may reach their verge of gravitational collapse may be written as

$$\langle n \rangle_{\text{crit}} = 70 \frac{(T_{\text{equiv}})^3}{(M/M_\odot)^2} . \tag{24}$$

The stronger the shock strength, the smaller the critical density and the greater the spectrum of large clouds that may be compressed beyond their verge of gravitational collapse in passage through the shock. For example, clouds of mass $M = 10^4\ M_\odot$ with an equivalent temperature $T_{\text{equiv}} = 300°$ K require a critical density of only about 19 H cm^{-3} for gravitational collapse under a shock of 8:1 strength. In their passage through the shock, all large clouds with a mean density $\langle n \rangle > \langle n \rangle_{\text{crit}}$ are likely candidates for young stellar associations, while less dense clouds will adjust into a new equilibrium.

Figure 12 illustrates what clouds may be placed on their verge of gravitational collapse by a shock of 8:1 strength. A cloud of a given mass that lies to the left of its critical curve will collapse under such a compression. On the other hand, if a cloud exhibits too much internal turbulence or is not of sufficient density, a shock of 8:1 strength is not

sufficient to place it on its verge of gravitational collapse. The "outlined box" in the figure indicates the region of (density, equivalent temperature)-space where most galactic gas clouds probably lie.

A process that may enhance the prospects for the collapse of a large gas cloud over a relatively long time period is the well-known process of accretion. All massive clouds and cloud complexes, which are large enough, tend to accrete more mass by inelastic collisions with smaller clouds and subclouds of smaller masses. Kahn (1968*b*) estimates that 50 million years may be a typical time scale for the evolution of gas clouds to their verge of gravitational collapse by accretion only (in a gaseous medium with mean density of about 1 H cm^{-3}). Yet, accretion by large clouds most certainly speeds up inside the shock region and in the subsonic region behind the shock. In this situation, the

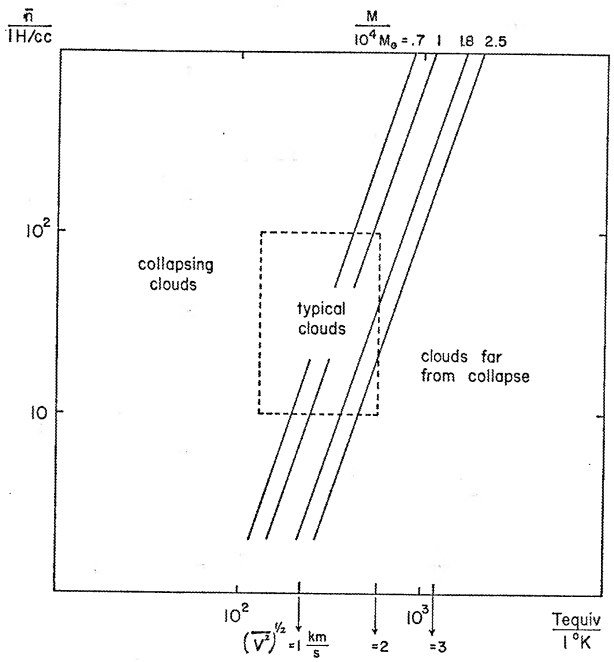

FIG. 12.—The collapse of gas clouds under an 8:1 shock compression. A cloud of a given mass that lies to the left of its critical curve will collapse under such a compression. A shock of the TASS pattern is of sufficient strength to place a gas cloud of typically large mass on its verge of gravitational collapse if its internal turbulence is not too large and if its density is not too small.

process of accretion, which acts to increase the mass of a large cloud throughout its prior journey before reaching the shock and especially in passage through the shock, combines with the galactic shock wave toward bringing about the gravitational collapse of the large cloud.

c) Stellar Associations

Because of internal turbulent eddies and fragments, the interior of the cloud may be visualized to consist of two distinct portions: (1) those regions consisting of clumps of gas concentration called subclouds, which are the candidates for protostars, and (2) the intersubcloud medium. Even though this model is somewhat of an idealization of the real physical picture, some basic features of star formation are apparent. In fact, the necessity for stellar associations in the cloud-subcloud picture is apparent. Since the amount of compression necessary for triggering the gravitational collapse of a gas concentration varies inversely with the square of its mass, it is much easier to trigger the gravitational collapse of a large cloud rather than a subcloud. Indeed, a shock with 8:1

strength may be capable of triggering the gravitational collapse of a typical large gas cloud; however, a compression on the order of *100000:1* is necessary to place a typical subcloud of mass $M = 50\,M_\odot$ and mean density $\langle n \rangle = 40$ H cm^{-3} on its verge of gravitational collapse. Therefore, an 8:1 shock wave compression can trigger *only* the collapse of the large cloud, which in turn is capable of triggering the subsequent compression and collapse of the individual subclouds. Each subcloud may form a star, and this newly born star lies in association with the stars formed from all the other subclouds inside the large cloud. The overall time for collapse of a typical large cloud from the shock-triggering stage to the formation of an association of newly born stars may be about 30 million years. It is inferred that subclouds can form stars only if they are contained in large clouds or in large cloud complexes. Moreover, newly born stars must practically always be found in associations with other newly born stars, and these newly born stellar associations for the most part must lie along spiral arms. These implications from the shock theory and the cloud model are already generally well established by observational studies.

V. DISCUSSION

a) Comparison with Earlier Work

At the time of Fujimoto's work on gas flow through a model spiral arm (1966), it was evidently not clear what a typical estimate of the pattern speed for our Milky Way system should be. In the absence of any a priori determination of the pattern speed, Fujimoto adopted a value of about 45 km sec^{-1} kpc^{-1}. This value presumably represents some kind of mean angular velocity of the matter in the galactic disk. A pattern speed of 12.5 km sec^{-1} kpc^{-1} determined from more recent observational studies[8] has been adopted in the present investigation.

One further major difference stands out between Fujimoto's calculations and the present investigation. A significant term of first order is neglected in each of Fujimoto's velocity component equations. These missing terms (present in eqs. [10] and [11] of this work) may be written

$$2(\Omega - \Omega_p)w_\parallel\,, \qquad -(\Omega - \Omega_p)w_\perp\,.$$

It should be noted that these terms are not negligible compared with other first-order terms such as $2\Omega_p w_\parallel$ and $2\Omega_p w_\perp$ when the flow region does not encompass the corotation neighborhood.

In summary, the basic physical differences between this analysis and Fujimoto's are:

1. Because of the high pattern speed, Fujimoto's calculations, which cover radii between 5 and 11 kpc, correspond to points lying outside corotation, which occurs at about 5 kpc in his model. In this work, the calculations for a pattern speed of 12.5 km sec^{-1} kpc^{-1}, which cover the radii between 3–4 and 12 kpc, correspond to points interior to corotation.
2. With the neglect of terms of $O(\Omega - \Omega_p)(w_\perp, w_\parallel)$, Fujimoto's analysis is valid to a good approximation only near corotation in his model. The results of the present investigation are valid to first order in the asymptotic approximation over the disk between 3–4 kpc and 12 kpc.
3. A two-armed spiral shock pattern covering a large portion of the galactic disk is obtained in the present work. No two-armed spiral shock pattern was obtained in Fujimoto's calculations.

b) Resultant Spiral Gravitational Field

The near coincidence of the spiral shock and of the peak of gas density with the center of the background spiral arm is an important feature in the TASS picture. Self-

[8] This pattern speed is obtained from two studies: (1) the distribution of neutral hydrogen, and (2) the migration of moderately young stars (see Lin, Yuan, and Shu 1969).

consistency requires that the induced field due to the response in the gaseous and stellar components be similar to the original imposed field that gives rise to the response. In the TASS picture, it is shown that the fundamental component of the nonlinear gas-induced field lies approximately in phase with the imposed field. Therefore, the imposed background spiral field may actually be regarded as the *resultant* spiral gravitational field of gas, young stars, and moderately old stars.

c) Narrow Star-Formation Regions

Attention may be focused on the narrowness of the gas-density peak located adjacent to the shock in Figure 6. Such a narrow peak in density and pressure indicates that appreciable star formation may take place only over the narrow spiral region lying just behind the large-scale galactic shock. During the time period for the formation and evolution of the relatively massive stars initiated at the shock (on the order of 30 million years), matter traverses a distance normal to the spiral arm of only about one-eighth the total wavelength separating successive arms. Therefore, the relatively massive and luminous newly born stars initiated in the peak of gas concentration at the shock are confined to the inner side of the observable gaseous spiral arm of H I; for, when they pass outside this region, they no longer are newly born or luminous. General agreement appears between this theoretical picture and observational studies of the Milky Way system that have provided evidence for the location of the newly-born stars and luminous H II regions for the most part along narrow spirals[9] and more recently on the inside of the gaseous spiral arms making up the grand design (Westerhout 1968).

d) H I *versus* H II *Distributions*

There is also general agreement with other observational features. M. S. Roberts (1967) has shown for a number of Sc-type galaxies that the optical arms lie significantly interior to the H I peak. Our own Milky Way system also exhibits this feature, as the Westerhout results (1958) for the distributions of H I and H II have confirmed. Since it would seem a priori that the distributions of H I and H II with respect to radius should have the same general character, with the peak of one coinciding with the peak of the other, the work of M. S. Roberts sheds a new light on the picture of spiral galaxies, namely, a large shift in the peak of H II away from the peak of H I seems to indicate a strong triggering mechanism that is capable of affecting the production of H II according to the mechanism's own pattern, considerably independent of the distribution of H I. This evidence then adds further support to a large-scale TASS pattern that can control to a large extent the star-formation process as well as the radial distribution of H II over the galactic disk.[10] In the Schmidt model of our own Milky Way system the calculations show that the TASS pattern extends outward to about a radius of 12–13 kpc and terminates there. Indeed, the reason why there may be no newly born stars and no H II regions coinciding with the regions of highest H I distribution in our own Galaxy and in many Sc-type galaxies may be that there are no shocks present at such large radii where the H I distribution is maximal.

e) Recent H II *Investigations*

We shall make one further comparison between the theoretical TASS picture and the recent observational studies of Kerr *et al.* (1968) on the distribution of H I and H II in the Galaxy.[11] They have drawn the following picture of the distribution of H II: Outside the nucleus and out to about 4 kpc, few H II regions can be found. At about 4 kpc many giant H II regions begin to appear, and from 4 to 6 kpc such H II regions are plentiful.

[9] See Morgan *et al.* (1952); Sharpless (1965).

[10] To be sure, the volume density of the gas could be lower because of reduced gravitational force perpendicular to the galactic plane in the outer parts of the Galaxy.

[11] See also Reifenstein 1968; Reifenstein *et al.* 1968.

They have found some H II in the 8-kpc region and smaller concentrations of H II in the solar neighborhood; however, the highest density of H II appears to be concentrated from 4 to 6 kpc (also see Westerhout 1958).[12] Moreover, the H II and H I arms that they have studied seem to coincide within a velocity difference of no greater than 10 km sec^{-1} from one another. These recently observed features even further indicate the general agreement between the TASS picture and observational studies of the Milky Way system.

I am very grateful to Dr. C. C. Lin for suggesting this problem to me and for his invaluable guidance and direction throughout this work. I would also like to thank Drs. F. D. Kahn, C. Hunter, and A. Toomre for their helpful advice and suggestions on various aspects of this work.

This work was supported in part by the National Science Foundation and the National Aeronautics and Space Administration. The numerical calculations were performed at the M.I.T. Computation Center.

REFERENCES

Axford, W. I. 1961, *Phil. Trans. Roy. Soc. London, A*, **253**, 301.
Baade, W., and Mayall, N. U. 1951, in *Problems of Cosmical Aerodynamics* (Dayton, Ohio: Control Air Documents Office), p. 165.
Barrett, A. H., Meeks, M. L., and Weinreb, S. 1964, *Nature*, **202**, 475.
Chandrasekhar, S. 1942, in *Principles of Stellar Dynamics* (New York: Dover Publishing Co.).
Clark, B. G., Radhakrishnan, V., and Wilson, R. W. 1962, *Ap. J.*, **135**, 151.
Ebert, R. 1955, *Zs. f. Ap.*, **37**, 217.
Field, G. B., Rather, J. D. G., Aannestad, P. A., and Orsag, S. A. 1968, *Ap. J.*, **151**, 953.
Fujimoto, M., 1966, in *I.A.U. Symp. No. 29* (in press).
Goldsworthy, F. A. 1961, *Phil. Trans. Roy. Soc. London, A*, **253**, 277.
Hunter, C. 1964, *Ap. J.*, **139**, 570.
———. 1967, *Am. Math. Soc. Lectures in Applied Mathematics*, **2**, 169.
Kahn, F. D. 1960, in *Die Entstehung von Sternen* (Berlin: Springer-Verlag), p. 104.
———. 1962, in *Interstellar Matter in Galaxies* (New York: W. A. Benjamin, Inc.), pp. 164–182.
———. 1968*a* (preprint, M.I.T.).
———. 1968*b* (personal communication).
Kahn, F. D., and Dyson, J. E., 1965, *Ann. Rev. Astr. and Ap.*, **3**, 47.
Kerr, F. J., Burke, B. F., Reifenstein, E. C., Wilson, T. L., and Mezger, P. G. 1968, *Nature*, **220**, 1210.
Kerr, F. J., and Westerhout, G. 1965, in *Galactic Structure* (Chicago: University of Chicago Press), p. 196.
Lasker, B. 1966*a*, *Ap. J.*, **143**, 700.
———. 1966*b*, *ibid.*, **146**, 471.
Lin, C. C. 1967, *Am. Math. Soc. Lectures in Applied Mathematics*, **2**, 66.
———. 1967, *Gen. Assembly IAU*, Prague.
Lin, C. C., and Shu, F. H. 1964, *Ap. J.*, **140**, 646.
———. 1966, *Proc. Nat. Acad. Sci.*, **55**, 229.
Lin, C. C., Yuan, C., and Shu, F. H. 1969, *Ap. J.*, **155**, 721.
Lindblad, B. 1963, *Stockholm Obs. Ann.*, **22**, 3.
Lindblad, B., and Langebartel, R. G. 1953, *Stockholm Obs. Ann.*, **17**, 6.
Lindblad, P. O. 1960, *Stockholm Obs. Ann.*, **21**, 3.
———. 1962, in *Interstellar Matter in Galaxies* (New York: W. A. Benjamin, Inc.), p. 222.
Mathews, W. G. 1965, *Ap. J.*, **142**, 1120.
Morgan, W. W., Sharpless, S., and Osterbrock, D. 1952, *A.J.*, **57**, 3.
Morgan, W. W., Strömgren, B., and Johnson, H. M. 1955, *Ap. J.*, **121**, 611.
Oort, J. H. 1962, in *Interstellar Matter in Galaxies* (New York: W. A. Benjamin, Inc.), pp. 3, 234.
———. 1965, *Gen. Assembly IAU, Hamburg*, p. 789.
Reifenstein, E. C. 1968, unpublished Ph.D. thesis, Massachusetts Institute of Technology.
Reifenstein, E. C., Wilson, T. L., Burke, B. F., and Mezger, P. G. 1968, A.A.S. meeting, Charlottesville, Va.
Roberts, M. S. 1957, *Pub. A.S.P.*, **69**, 59.
———. 1962, *A.J.*, **67**, 437.
———. 1967, Gen. Assembly IAU, Prague.

[12] Star formation triggered by the TASS pattern is predicted to be most prominent near 4 kpc in the galactic disk (see § III*a*).

Roberts, W. W. 1968*a*, A.A.S. meeting, Charlottesville, Va.
———. 1968*b*, unpublished Ph.D. thesis, Massachusetts Institute of Technology.
Sandage, A. 1961, in *The Hubble Atlas of Galaxies* (Washington, D.C.: Stinehour Press).
Schmidt, M. 1965, in *Galactic Structure* (Chicago: University of Chicago Press), p. 513.
Sharpless, S. 1965, in *Galactic Structure* (Chicago: University of Chicago Press), p. 131.
Spitzer, L. 1962, in *Interstellar Matter in Galaxies* (New York: W. A. Benjamin, Inc.), p. 98.
———. 1968, in *Nebulae and Interstellar Matter* (Chicago: University of Chicago Press), Vol. 1.
Wentzel, D. G. 1966, *Ap. J.*, **145**, 595.
Westerhout, G. 1958, *B.A.N.*, **14**, 215 and 261.
———. 1968 (personal communication).
Yuan, C. 1969 (to be published).